(Received 13 December 2025, Accepted 26 January 2026, Scheduled 12 March 2026)

Enhanced Gain Ultra-Wideband Antenna with Different Notch Response

Mohammed F. Hasan[1], Hussein Al-Jeshami[2], Hussam Al-Saedi[1,*], Hussain A. Hammas[1], Muhannad Y. Muhsin[3], and Jawad K. Ali[1]

[1] *College of Communication Engineering, University of Technology, Iraq*
[2] *College of Electromechanical Engineering, University of Technology, Iraq*
[3] *College of Electrical Engineering, University of Technology, Iraq*

ABSTRACT: This article presents an enhanced-gain ultra-wideband (UWB) antenna with multiple notch responses to suppress the effects of coexisting wireless systems. The proposed antenna is developed in two stages. In the first stage, a reduced-ground U-shaped monopole with parasitic patches was designed to obtain a wide bandwidth between 3.02 and 10.76 GHz while maintaining a peak realized gain higher than 7 dB. In the second stage, selective frequency-rejection capabilities are tuned using split-ring structures (SRSs) for dual and higher-order notch responses. Two configurations are studied: dual-set SRS, which gives rise to low and high region notches centered at 5.73 GHz and 8.31 GHz, respectively, and higher-order SRS notch configuration providing a broad notch about 6.78 GHz with a 5.45% fractional rejection bandwidth. Parametric analysis indicated that the notch depth, notch bandwidth, and center frequency were independent and could be controlled via geometric tuning. The simulated results, supported by measurements from Keysight's PNA-X, corroborate the reflection coefficient, gain behavior, and notch performance; any deviations are attributed to variations experienced during the fabrication. The proposed approach achieves a UWB, increased gain, and flexible interference suppression, qualifying it for modern UWB communication systems that require a compact design.

1. INTRODUCTION

Antenna is an important part of any wireless system. It can be employed in many systems where sensing technology or link communication is required. There are many types of antennas; their shapes and types depend on the required performance and their task. Ultra-wideband (UWB) communication systems have received increasing attention in recent years due to their ability to support high data rates, low power consumption, and robustness against multipath fading. Since the Federal Communications Commission (FCC) authorized the 3.1–10.6 GHz frequency range for unlicensed UWB operation [1], numerous research efforts have focused on developing efficient UWB antennas for diverse applications, including wireless communications [2, 3], microwave imaging [4, 5], positioning, vehicular systems [6], and wearable electronics [7, 8]. These applications require antennas with compact size, stable radiation patterns, high gain, and wide impedance bandwidth [9]. Despite their advantages, UWB antennas have several challenges. The inherently wide operating bandwidth often leads to variations in radiation characteristics, reduced gain at upper frequencies, and increased susceptibility to interference from narrowband services, such as WLAN (5–6 GHz), WiMAX, and emerging sub-6 GHz 5G systems. Consequently, notch-band capabilities have become essential for improving immunity against coexisting wireless systems [10, 11]. Furthermore, gain enhancement remains a persistent challenge [12], especially for compact planar antennas intended for portable or embedded systems. Achieving high gain together with selective notch-band rejection requires a careful balance among geometry modification, resonant loading, and ground-plane engineering. The design must suppress specific interfering bands while ensuring minimal distortion of the transmitted UWB pulses, particularly for applications such as biomedical imaging and high-resolution radar systems. Recent research has shown that integrating parasitic elements, fractal features, slots, stubs, artificial magnetic conductor (AMC) layers, and reconfigurable structures can significantly improve the performance of UWB antennas; however, each approach has limitations in size, complexity, or gain stability. Given these challenges, this paper aims to develop an enhanced-gain UWB antenna with different notch responses, providing improved radiation characteristics and better interference mitigation compared with conventional UWB antenna designs.

2. RELATED WORK

Several UWB antenna designs have been proposed to address bandwidth widening, gain enhancement, and interference suppression [13]. Printed monopole antennas remain a popular choice because of their simple structure, low cost, ease of integration, and ability to achieve a wide bandwidth. For example, a jug-shaped coplanar waveguide (CPW)-fed printed monopole antenna was introduced in [14], covering 3.02–10.76 GHz by employing parasitic elements and ground-plane reduction to improve impedance matching. Similarly, a compact UWB planar monopole antenna with a ribbon-shaped slot was designed in [15], where the insertion of a novel radiator slot and CPW ground (CPWG) vias enhanced the opera-

* Corresponding author: Hussam Al-Saedi (hussam.h.ali@uotechnology.edu.iq).

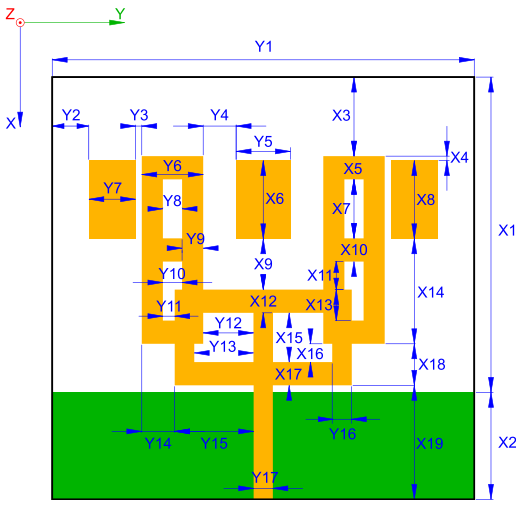

FIGURE 1. Proposed antenna with dimension annotations.

tional bandwidth and produced stable omnidirectional radiation patterns. In biomedical applications, particularly microwave imaging, UWB antennas must ensure stable time-domain behavior, constant radiation characteristics, and sufficient penetration depth. A pentagonal fractal CPW-fed antenna achieving a bandwidth of 3–12.7 GHz with stable group delay performance was reported in [16], demonstrating suitability for imaging systems. Likewise, a slotted UWB monopole antenna with a truncated ground plane was proposed in [17], achieving 141% fractional bandwidth (FBW) and improved gain due to the optimized slot geometries. Ultra-thin and compact structures have also emerged, as illustrated in [18], where an ultra-thin UWB microstrip antenna incorporated feed-line tuning and incomplete ground characteristics to maintain stable performance in wearable imaging scenarios. Several notch-generation techniques have been explored to mitigate the interference from narrowband systems inside the UWB spectrum. Reconfigurable approaches using radio frequency microelectromechanical system (RF-MEMS) switches have shown promise, enabling the dynamic selection of notched bands while retaining ultra-wideband operation. For instance, the design in [19] demonstrated a tunable notch around 5–6 GHz with an enhanced peak gain (9 dBi) by integrating MEMS-controlled resonant structures with CPW feeding. However, these designs often introduce complexity and increase the fabrication costs. Textile and wearable antennas have integrated artificial magnetic conducting (AMC) surfaces to reduce the specific absorption rate (SAR) and enhance the gain. An all-textile UWB monopole coupled with an AMC reflector in [20] achieved a maximum gain of 9.67 dBi and significantly reduced SAR values, highlighting the potential of artificial surfaces for gain enhancement. Nevertheless, AMC-based antennas typically require a larger footprint due to their arrayed unit cells. Multiple-input multiple-output (MIMO) antennas further extend UWB capabilities by improving isolation, diversity, and gain. The compact 2×2 UWB MIMO antenna in [21] achieved bandwidths from 3.28 to 17.8 GHz with mutual coupling below -20 dB and a consistent gain above 2 dBi. Comprehensive reviews of UWB antenna development, such as the systematic analysis in [22], highlight the ongoing challenges in achieving compactness, high gain, interference rejection, and radiation stability. These studies collectively demonstrate that although significant progress has been made in UWB bandwidth enhancement and specialized applications, there remains a clear need for compact antennas capable of simultaneously providing enhanced gain and flexible notch-band responses to provide coexistence capability with other ISM wireless systems.

TABLE 1. Geometric dimensions, all in mm.

Dim	Value	Dim	Value	Dim	Value	Dim	Value
Y1	36.67	Y10	1.67	X2	9.29	X11	2.43
Y2	3.17	Y11	1.03	X3	6.86	X12	2.02
Y3	0.53	Y12	4.37	X4	0.39	X13	2.69
Y4	2.86	Y13	5.14	X5	2.02	X14	9.12
Y5	4.71	Y14	2.86	X6	6.79	X15	4.28
Y6	5.34	Y15	6.86	X7	5.12	X16	1.59
Y7	4.07	Y16	1.7	X8	6.79	X17	2.02
Y8	1.67	Y17	1.67	X9	4.41	X18	3.61
Y9	1.83	X1	27.38	X10	2.02	X19	9.90

3. THE PROPOSED METHOD

In this study, two designs were proposed: design #1 (D1) and design #2 (D2). The geometric dimensions, parametric studies, and simulation-based results for each design are presented in the following subsections. Moreover, Subsection 3.3 shows the validations and measurement results.

3.1. Antenna Design of D1

The frequency spectrum allocation for an ultra-wideband antenna (UWBA) typically ranges from 3.1 GHz to 10.6 GHz [1]. The proposed antenna in this research is based on a reduced ground structure and illustrated in Fig. 1. Its geometric dimensions are listed in Table 1. The antenna is constructed from two types of patches: the main U-shaped patch and the center and side parasitic patches. The use of the net-shaped structure helps in routing the surface current, thus generating the required propagation mode for the proposed design. Additionally, small patches were employed to enhance the antenna's directivity within its operating frequency band (OFB). A Rogers 4350 substrate with a relative permittivity of 3.66, loss tangent of 0.0037, and height of 0.762 mm was used to implement the antenna design.

3.1.1. Parametric Study of D1

To investigate the impact of antenna dimensions on performance, a series of parametric studies was conducted. The dimensions of Y3, X2, and Y8 had the greatest effect on the antenna. The variations in each dimension are shown in Figs. 2, 3, and 4. It can be concluded that increasing Y3 from 0.5 mm to 2.5 mm improves the matching of the antenna (S_{11} changes from -10 to -13), that is, a better reflection coefficient (S_{11}) effect. Additionally, a wider operational frequency range can

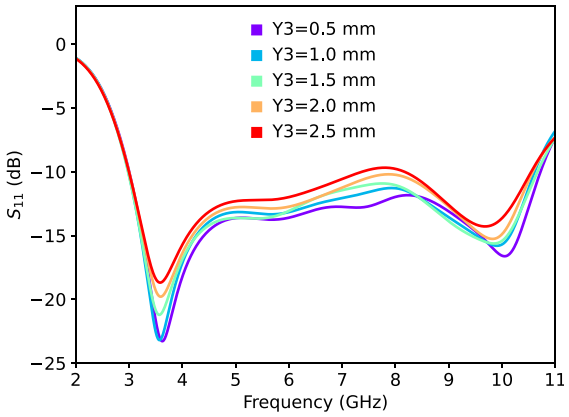

FIGURE 2. Parametric study effect of Y3 on reflection coefficient.

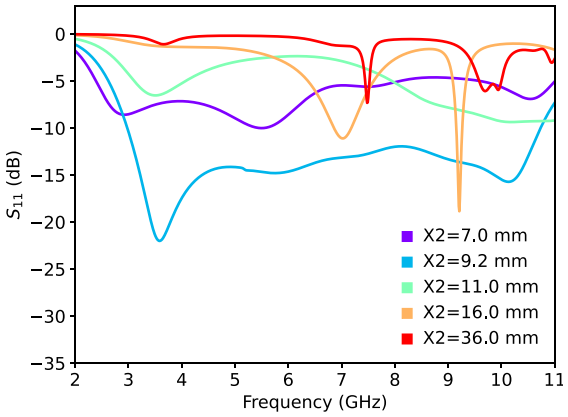

FIGURE 3. Reduced-ground effect by X2 variations.

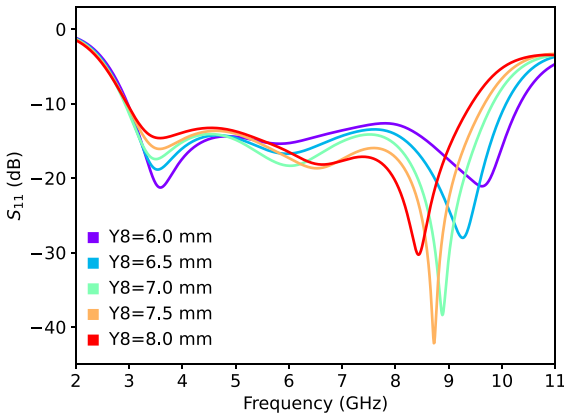

FIGURE 4. Upper frequency shifting by Y8 variations.

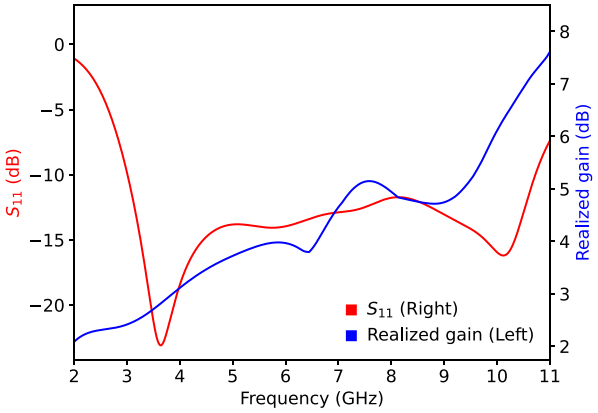

FIGURE 5. Reflection coefficient and peak realized gain of D1.

be achieved by reducing the ground plane (X2), from near 1 GHz at 36 mm to 8 GHz at 7 mm. The optimal value for the proposed antenna was found to be 9.29 mm. Furthermore, increasing Y8 from 6 mm to 8 mm leads to shifting the upper cutoff frequency of the antenna from 9.8 GHz to 8.3 GHz, respectively, with a negligible shift in the lower cutoff frequency of the designed antenna.

3.1.2. Performance of D1

A full-wave simulator, Ansys EDT (AEDT), was used to simulate the D1 performance. Fig. 5 shows D1's reflection coefficient and peak realized gain. It can be concluded that S_{11} is better than 11.8 dB, where the resultin -10 dB OFB spans from 3.02 GHz to 10.76 GHz. Additionally, the gain performance of D1 ranges from 2 dBi to 7 dBi.

To plot the electric field distribution (EFD) of the UWBA, three different frequencies within the OFB were selected. They are 3.1 GHz, 6.0 GHz, and 10.7 GHz, and the associated EFDs are shown in Fig. 6. It can be noted that at 3.1 GHz, the EFD is mainly concentrated with fair intensity along the radiating edges of the main patch and the lower edge of the antenna structure. In comparison, at 6.0 GHz, the EFD became more concentrated and intense along the lower edge of the antenna. However, the EFD changed significantly when the most intense electric fields were located at the upper corners of the main patch and at the corners near the lower edge of the antenna. At this frequency, it can also be noted that the EFD, in comparison with the EFDs at other frequencies, has more intensity along the upper arms of the main patch. In addition, Fig. 7 exhibits the normalized radiation patterns in the E and H planes of D1 at the same frequencies used for plotting the EFDs.

It should be pointed out that the radiation pattern at 3.1 GHz is bidirectional and dumbbell-shaped in the E-plane, with the main lobe directed towards the boresight, while the H-plane pattern is highly symmetrical. At this frequency, the cross-polarization (X-Pol) levels are very low in both planes, remaining below -30 dB, indicating excellent performance. Additionally, at 6.0 GHz, the antenna maintains almost the same pattern in the E and H planes as in 3.1 GHz but with higher X-Pol levels. However, X-Pol is still fairly below -10 dB, demonstrating good performance. Moreover, the radiation patterns show significant degradation at 10.7 GHz with a considerable increment in the side-lobe levels, leading to a less uniform pattern formed in the H-plane. Compared to the lower frequencies, the X-Pol levels are notably increased, suggesting a deterioration in the performance at the upper end of the antenna's OFB.

3.2. Antenna Design of D2

To coexist with other wireless communication systems, a notch response is required to eliminate the interference from these

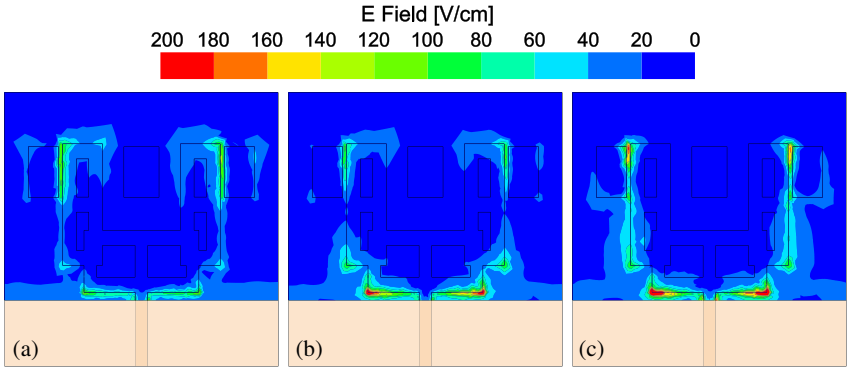

FIGURE 6. Field distributions of D1 at selected frequencies. (a) 3.1 GHz, (b) 6.0 GHz, (c) 10.7 GHz.

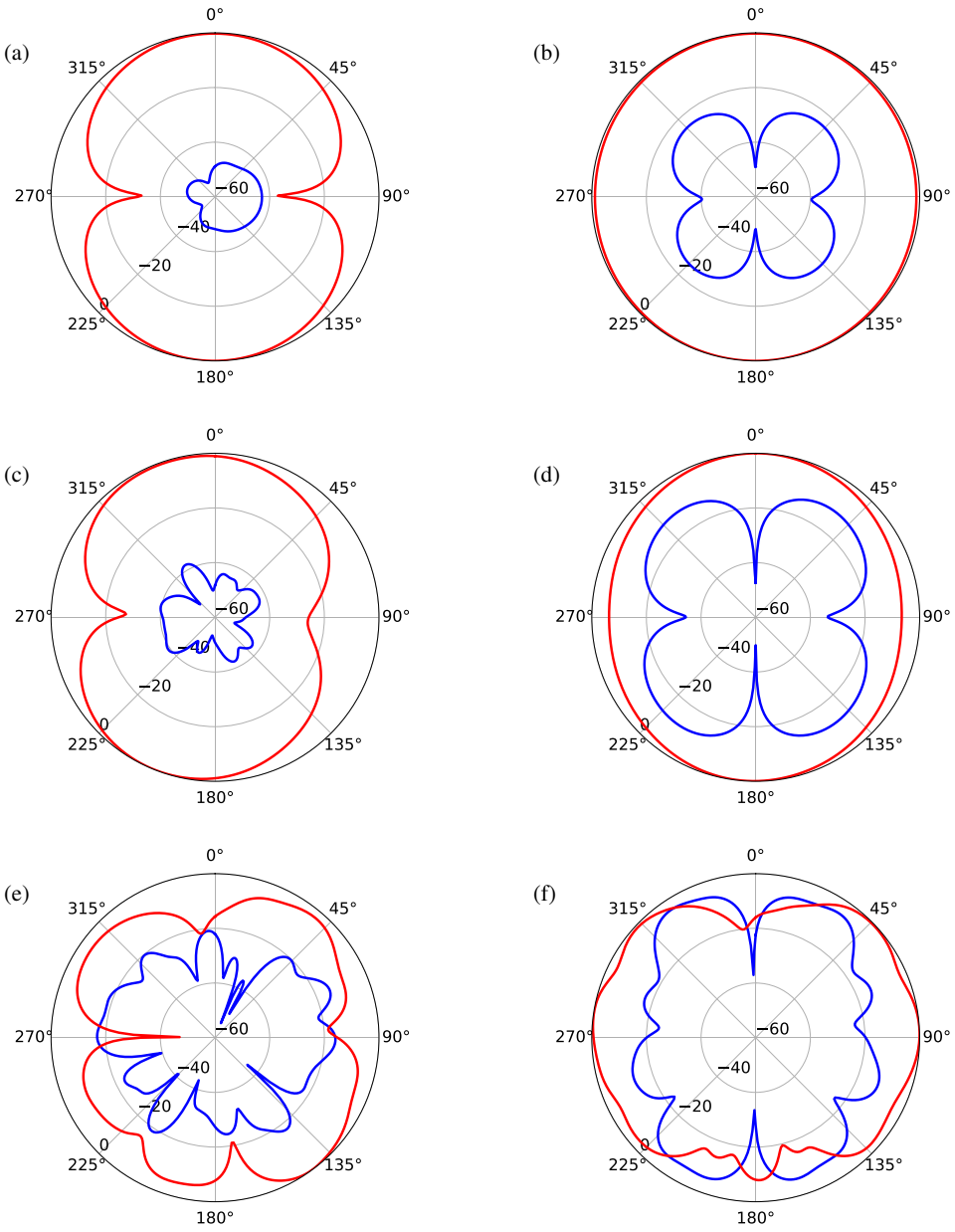

FIGURE 7. Normalized radiation patterns in E and H planes for D1 at various frequencies. Red is the co-polarization, while blue is the cross-polarization. (a) E-plane at 3.1 GHz, (b) H-plane at 3.1 GHz, (c) E-plane at 6.0 GHz, (d) H-plane at 6.0 GHz, (e) E-plane at 10.7 GHz, (f) H-plane at 10.7 GHz.

TABLE 2. D2C1 dimensions, all in mm, where a and b denote the parts of the dual-set to which the dimension belongs.

Dim	Value	Dim	Value	Dim	Value	Dim	Value
sY1a	4	sX1a	0.25	sY1b	3	sX1b	0.25
sY2a	0.3	sX2a	0.25	sY2b	0.3	sX2b	0.25
sY3a	0.3	sX3a	0.25	sY3b	0.3	sX3b	0.25
sY4	0.14	sY5	0.14	sX4	1.155	sX5	0.2

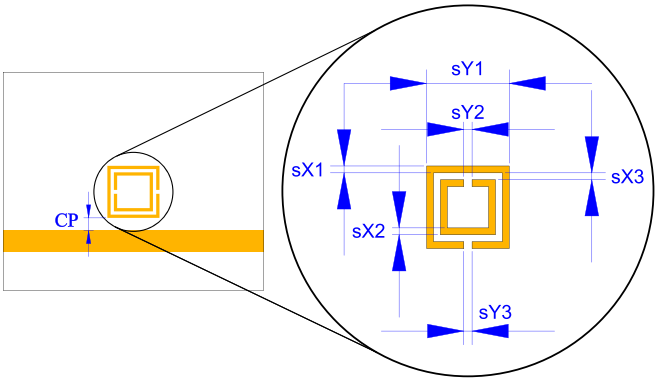

FIGURE 8. Notch filter using split-ring resonator.

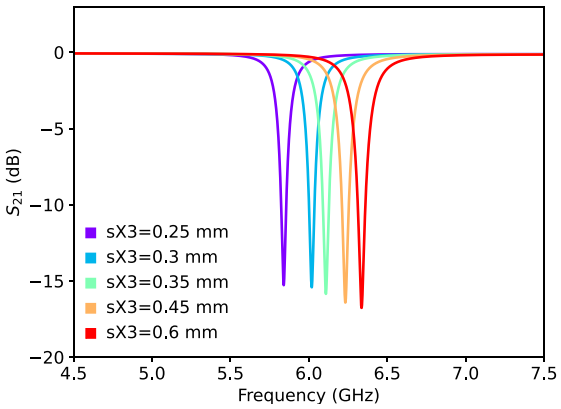

FIGURE 9. Controlling center frequency using sX3.

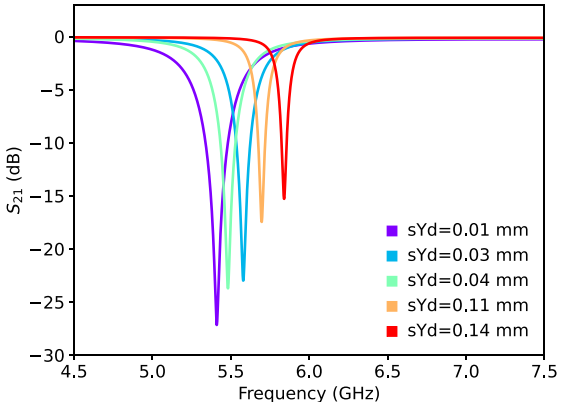

FIGURE 10. Controlling bandwidth using coupling factor.

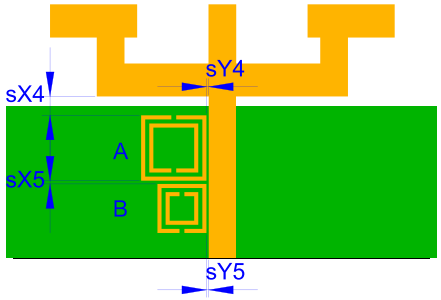

FIGURE 11. SRS employment in D2C1.

systems. This can be achieved by integrating a notch filter within the antenna's response. In this paper, the notch response was generated using a split-ring structure (SRS). The SRS was designed using filter design theory as in [23]. It can be understood that loading a microstrip line with an SRS leads to a notch filter realization. This is because SRS behaves as a short-loaded resonator. Moreover, the response of the notch filter can be controlled by setting the size, number of SRSs, and the coupling gap with the microstrip line. The basic SRS that is employed in D2 is illustrated in Fig. 8. Parametric studies were done to ensure that SRS fit the needs of adaptability to block any signal at certain frequency. The resonance frequency of the SRS can be set by controlling sX3 as shown in Fig. 9, while the bandwidth of the notch can be set using the coupling factor (CP) between the SRS and the feed line as shown in Fig. 10. For D2, two cases were introduced: in the first case (D2C1), two notches were generated using two different SRSs, while in the second case (D2C2), a wide band notch was achieved using multiple SRSs with the same size. In the following subsections, D2C1 and D2C2 will be discussed in detail.

3.2.1. Antenna Design of D2C1

In this case, the antenna feed was loaded by a dual-set SRS. Fig. 11 shows the location and parameters used in configuring D2C1, and the dual-set in this case is divided into two parts: A and B, where each has its own dimensions denotation with respect to the basic SRS parameters in Fig. 8. Table 2 lists the dimensions used in D2C1. These two parts generate two notch responses, a low-region notch (LRN) and a high-region notch (HRN), each of which has its own center frequency due to the different dimensions used between the two parts of the dual-set.

3.2.2. Parametric Study in D2C1

To determine which dimensions change the characteristics of the notches in this case, parametric studies were performed,

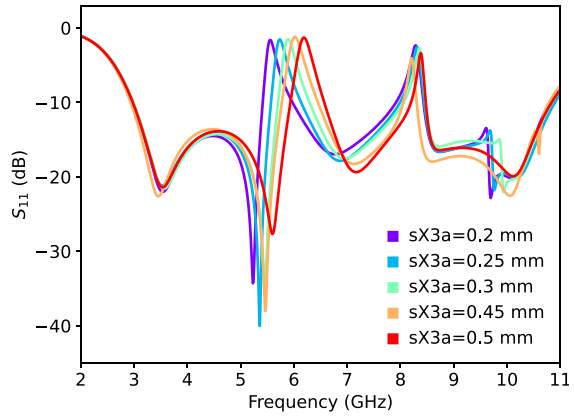

FIGURE 12. Effect of changing sX3a on LRN.

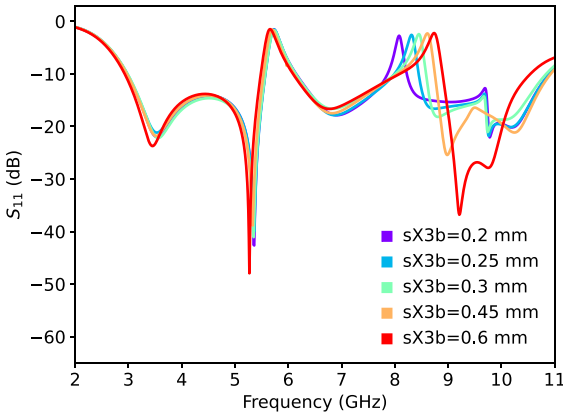

FIGURE 13. Effect of changing sX3b on HRN.

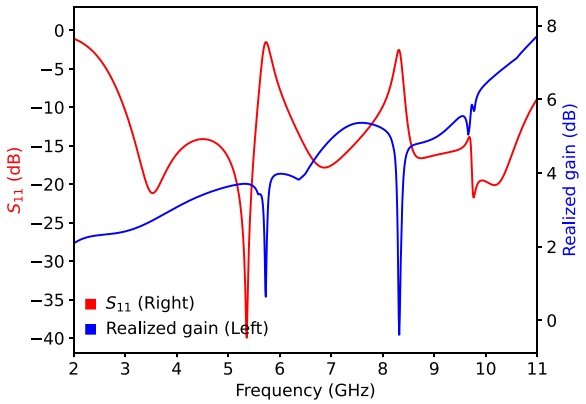

FIGURE 14. Reflection coefficient and peak realized gain of D2C1.

and it is found that sX3a and sX3b have the most impact on notch performance. Increasing sX3a from 0.2 mm to 0.5 mm leads to shifting the LRN response to a higher frequency from 5.5 GHz to 6.4 GHz as shown in Fig. 12; additionally, increasing sX3b from 0.2 mm to 0.6 mm leads to a shift in the HRN response from 8 GHz to 8.8 GHz as demonstrated in Fig. 13. Both Figs. 12 and 13 prove that the two notches can be independently designed and controlled.

3.2.3. Performance in D2C1

The simulation results for this case are presented in Fig. 14. In this case, the first notch is centered around 5.73 GHz with an FBW of 2.44%, S_{11} of -1.5 dB, and almost 0 dBi gain, while the second notch is centered around 8.31 GHz with an FBW of 0.72%, S_{11} of -2.5 dB, and 0 dBi gain. It can also be concluded that S_{11} was lower than -14 dB across the OFB. Moreover, the lower cutoff frequency of the OFB is shifted from 3.02 GHz (as in D1) to 2.98 GHz; on the other hand, the upper cutoff frequency is shifted from 10.76 GHz (as in D1) to 10.9 GHz. This means that employing notch responses leads to 180 MHz more bandwidth. Furthermore, Fig. 15 illustrates that the D2C1 antenna has no radiating field at the center frequencies of the generated notches. This is due to the effect of SRS loading on the feed line.

3.2.4. Antenna Design of D2C2

In this case, a broad notch response is generated using a higher-order notch filter. This is done using two dual-set SRSs to load the feed of the antenna. Fig. 16 shows the configuration of this case, where its dimensions are illustrated in Table 3.

TABLE 3. D2C2 dimensions, all in mm.

Dim	Value	Dim	Value	Dim	Value
sY1	3.4	sX1	0.25	sX6	0.85
sY2	0.25	sX2	0.25	sX7	1.4
sY3	0.25	sX3	0.25	sY6	0.3

3.2.5. Parametric Study in D2C2

Parametric studies were done to control the notch response characteristics, thereby changing the notch transmission zero (NTZ), center frequency (NCF), and bandwidth (NBW). The NTZ is affected by variations in sX6. Fig. 17 depicts that the depth of NTZ is improved by increasing sX6 from 0.1 mm to 0.55. On the other hand, increasing sY1 from 2.8 mm to 3.6 mm relocates NCF to a lower frequency as shown in Fig. 18. Moreover, lowering values of sY6 from 0.16 mm to 0.02 mm produces higher NBW (0.8 GHz to 2 GHz), which, however, has a negative impact on the selectivity of the notch response as demonstrated in Fig. 19.

3.2.6. Performance in D2C2

To fully evaluate the design capability in this case, the S_{11} and maximum realized gain results were simulated. Fig. 20 shows D2C2's performance as the OFB ranges from 2.98 GHz to 10.92 GHz with S_{11} less than -14 dB, except for the notch region which has a center frequency of 6.78 GHz and FBW of 5.45%. It can also be concluded from Fig. 21 that D2C2 does not radiate any signal in the notch region. Furthermore, the peak realized gain in Fig. 20 clarifies that the maximum realized gain was up to 7 dB in the OFB. It can also be concluded that the antenna's gain in the notch region is severely dropped below 0 dBi.

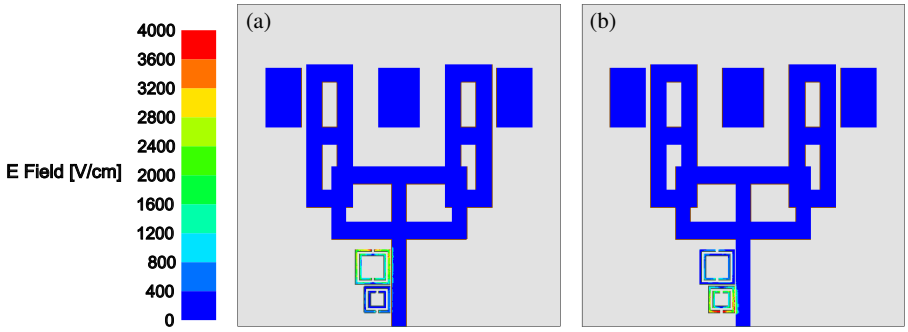

FIGURE 15. Fields distribution of D2C1 at notch CFs. (a) 5.73 GHz, (b) 8.31 GHz.

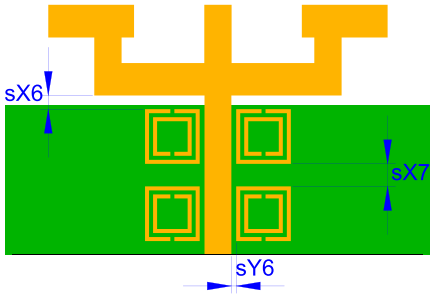

FIGURE 16. SRS employment in D2C2.

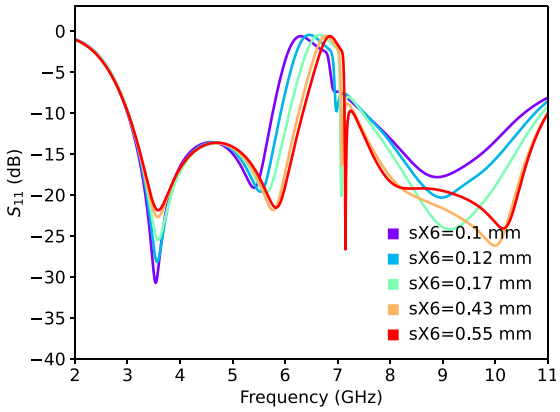

FIGURE 17. D2C2: NTZ performance vs sX6.

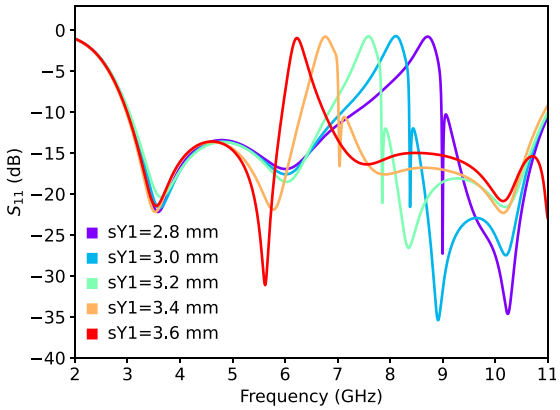

FIGURE 18. D2C2: NCF location vs sY1.

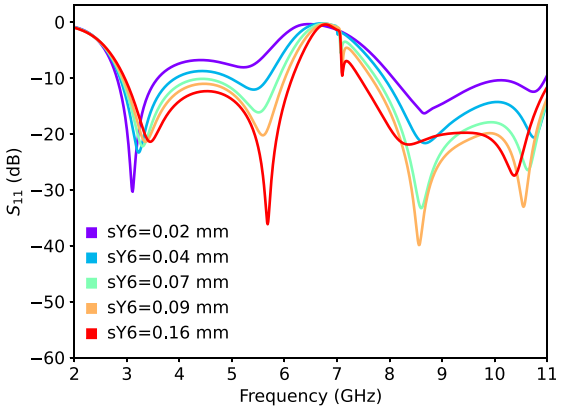

FIGURE 19. D2C2: NBW impact by sY6.

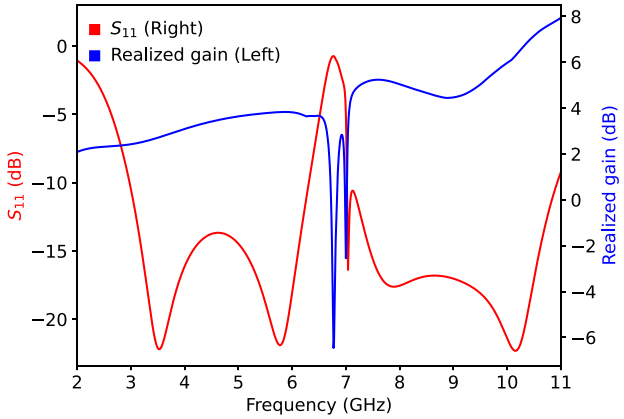

FIGURE 20. Reflection coefficient and peak realized gain of D2C2.

3.3. Time Domain Analysis of the Proposed Designs

Ideally, to avoid signal dispersion where all pulse frequency components are transmitted at the same time, the group delay (GD) of the UWB antenna must maintain a flat and constant value. Fig. 22 shows the GD of D1, D2C1, and D2C2, where D1's GD (red) indicates linear phase behavior. However, in both cases of D2, it can be inferred that distinct spikes are presented. For D2C1, both GD spikes are located at the center frequencies of the notch regions. It confirms the presence of band-stop behavior near 5.73 GHz and 8.31 GHz. Additionally, in the case of D2C2, a larger and wider spike of GD is

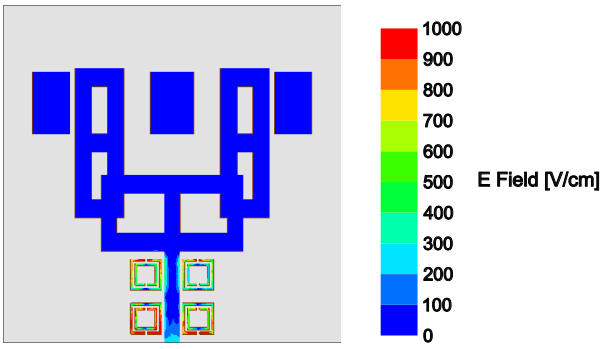

FIGURE 21. Fields distribution of D2C2 at 6.78 GHz.

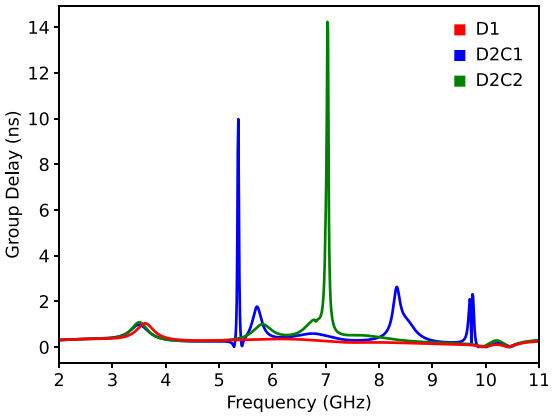

FIGURE 22. Group delay for D1, D2C1, and D2C2.

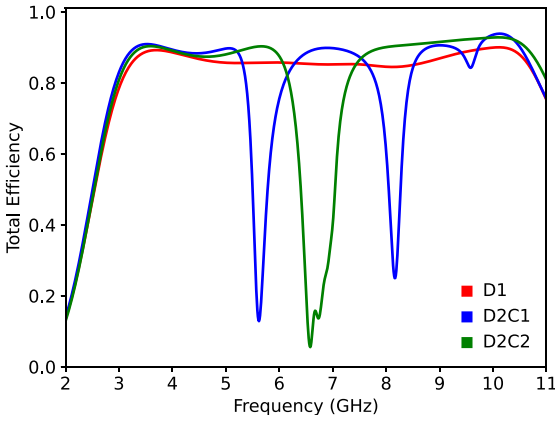

FIGURE 23. Total efficiency for D1, D2C1, and D2C2.

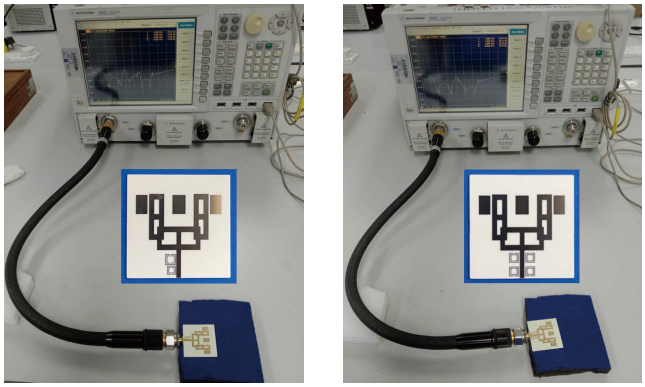

FIGURE 24. Measurement setups for D2C1 and D2C2.

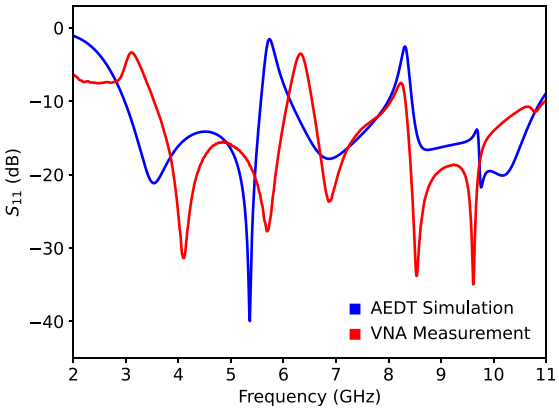

FIGURE 25. Reflection coefficient validation of D2C1.

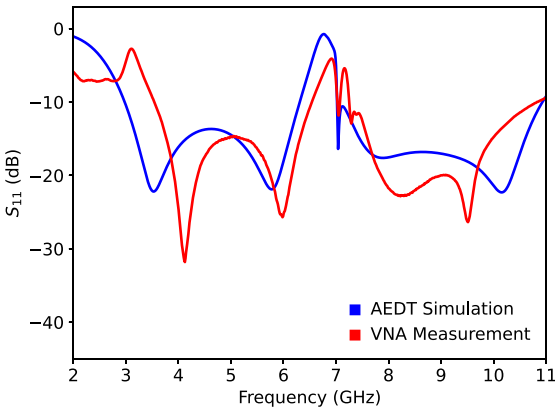

FIGURE 26. Reflection coefficient validation of D2C2.

presented within the notch region. It correlates to the sharpness of the generated rejection notch.

3.4. Efficiency of the Proposed Designs

To validate the gain performance of the proposed antenna, efficiency results were simulated. The efficiency helps verifying if the antenna performance was pushed to its physical and loss-limited bounds. Fig. 23 illustrates the antenna's total efficiency, taking into consideration the material losses in the antenna and the reflection effect at its input. It can be concluded that the three proposed designs exhibit high efficiency across the OFB up to 90%, which confirms a good radiation performance. Additionally, since intentional band-notches were introduced in D2C1 and D2C2, it can be noticed that the efficiency went down to 20%, which correlates with the results of the realized gain and S_{11}.

3.5. Measurements and Results Validation

To validate the simulation results of the proposed designs, a measurement setup was made using a Keysight PNA-X network analyzer (N5242A). Fig. 24 shows the measurement setups for D2. The validation results are highlighted in Figs. 25 and 26, respectively. These figures successfully validate the

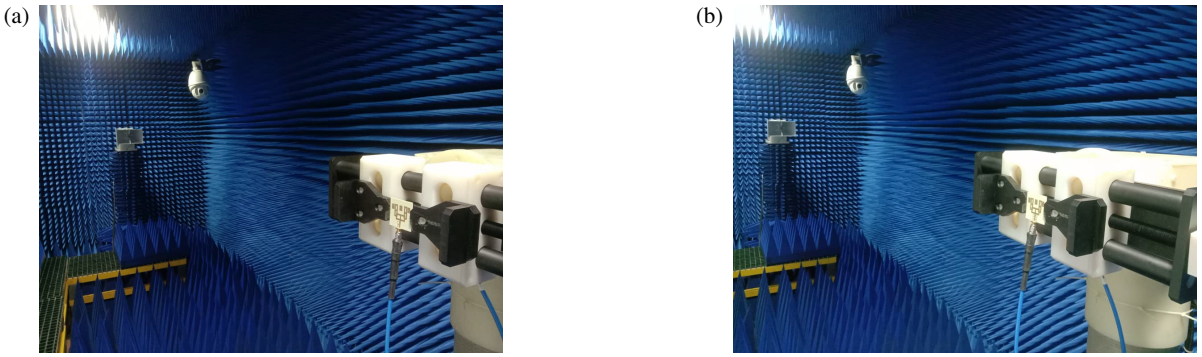

FIGURE 27. Far-field anechoic chamber measurement setup D2 cases. (a) D2C1, (b) D2C2.

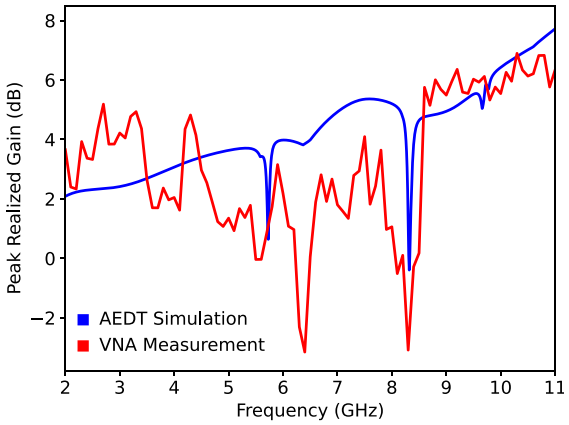

FIGURE 28. Peak gain validation of D2C1.

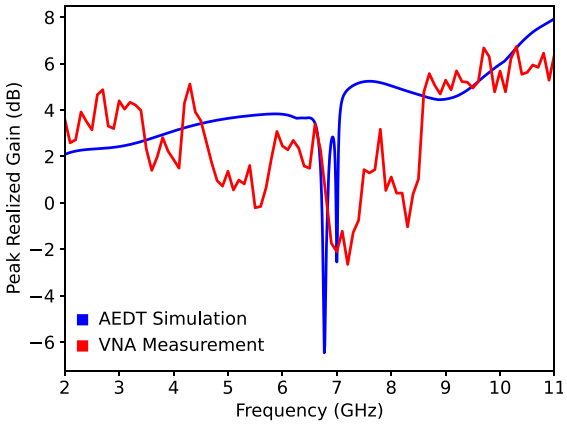

FIGURE 29. Peak realized gain validation of D2C2.

two D2 cases by comparing the simulated (AEDT) and measured (VNA) S_{11} findings. For both cases, there is a strong overall agreement between the simulation and the measurement, confirming that the antenna cases achieve an ultra OFB with S_{11} well below the required -10 dB threshold for antenna design. While the overall performance aligned very well, minor and expected discrepancies were noted, such as slight frequency shifting and differences in depth at the TZs. These types of small variations are typically common because of fabrication tolerances, material property standard deviations, and calibration quality in the measurement setup; however, the strong correlation between the AEDT and VNA results verifies the performance of the fabricated antenna and the accuracy of the simulation models.

To validate the simulation results, far-field anechoic chamber measurement setups were utilized to evaluate the realized gain of D2C1 and D2C2 using a standard-gain horn antenna, as shown in Fig. 27. Keysight ENA E5071C was used in the measurement setup with 91 sweep points of a frequency range from 2 GHz to 11 GHz. Additionally, 10-degree stepped elevation and azimuth angles were utilized in $0°$–$360°$ and $0°$–$180°$, respectively. The comparison between the simulated and measured gains of D2C1 is shown in Figs. 28 and 29. Both AEDT and VNA results show that the gain generally increases with frequency. However, the measured gain was consistently lower than the simulated one and exhibited more significant fluctuations or ripples. Additionally, the notches appear deeper in measurement than in simulation results for D2C1 as shown in Fig. 28.

Measurement validations in D2C1 and D2C2 indicate a very wide operational bandwidth (2.98–10.90 GHz), good notch behavior, and gain performance for the antenna. Measurement uncertainties, such as small frequency shifts and gain reductions, may be attributed to the expected fabrication limits, material tolerances, and connector and cable losses. Overall, and the proposed antenna designs exhibit high gain, compact geometry, and versatile suppression of unwanted bands, thus forming a strong candidate for UWB applications in short-range communications, radar sensing, and integrated multi-band wireless devices.

The proposed antenna designs (D1, D2C1, and D2C2) demonstrated a superior balance of performance characteristics compared to the cited literature, particularly in terms of peak realized gain and compactness as listed in Table 4. Although references such as [16, 18, 20] offer wider bandwidths (up to 9.82 GHz), they exhibit significantly lower peak gains, ranging between 3.6 and 4.4 dBi. In contrast, the proposed designs achieved substantially higher gains of 7.2 to 7.8 dBi, outperforming the highest gain among the references ([23] at 6.6 dBi). Furthermore, this performance is achieved with a highly compact footprint; design D1 ($0.0023\lambda_g^3$) is smaller than most references, and even the notched designs (D2C1 and D2C2) are roughly three times smaller than the closest gain competitors [17, 24], which possess sizes of roughly $0.01\lambda_g^3$.

TABLE 4. Comparison with literature, where BW is bandwidth; CF is center frequency; MG is maximum realized gain within the OFB. Size was calculated with respect to λ_g (guided wavelength at the lowest frequency of antenna's OFB).

Ref.	BW (GHz)	CF (GHz)	MG (dBi)	Notch Count	Size (λ_g^3)
[14]	8	7	4.1	0	0.0052
[15]	7.7	6.95	4	0	0.0021
[16]	9.7	7.85	3.6	0	0.0015
[17]	8.72	7.56	6.43	0	0.0103
[18]	8.9	7.55	4.4	0	0.0012
[20]	9.82	8.09	4	0	0.0025
[24]	8.7	7.05	6.6	0	0.0097
D1	7.7	6.86	7.2	0	0.0023
D2C1	7.92	6.94	7.5	2	0.0031
D2C2	7.92	6.94	7.8	1	0.0031

4. CONCLUSION

In this study, an enhanced gain UWB antenna integrated with tunable notch-generation mechanisms to control interference was introduced. Beginning from a reduced-ground structure, a wide -10 dB impedance bandwidth and stable gain characteristics across the operational UWB range were achieved. The controlled employment of both dual and higher order notch responses was realized using split-ring resonator structures. From parametric studies, it was confirmed that the resonator dimensions influence the notch center frequency, depth, and bandwidth, thereby providing a flexible method for customizing the interference-rejection characteristics set for various wireless standards. Future studies may extend this design to reconfigurable or adaptive notch structures to further promote dynamic spectrum coexistence.

REFERENCES

[1] "Revision of Part 15 of the commission's rules regarding ultra wideband transmission systems," Tech. Rep. FCC 02-48, eT Docket No. 98-153; 17 FCC Rcd 7435, Federal Communications Commission, Washington, D.C., Apr. 2002.

[2] Yao, S., T. Yang, X. Qiu, and X. Li, "A frog-shaped UWB MIMO antenna design for 5G," *Progress In Electromagnetics Research C*, Vol. 151, 101–112, 2025.

[3] Yao, S., X. Qiu, and T. Yang, "A miniaturized UWB MIMO antenna design for 5G multi-band applications," *Progress In Electromagnetics Research C*, Vol. 153, 1–12, 2025.

[4] Sekhar, M. and N. Suman, "CPW fed super-wideband antenna for microwave imaging application," *Progress In Electromagnetics Research C*, Vol. 130, 201–212, 2023.

[5] Singh, C. and C. Sharma, "A miniaturized SC-DGS tapered-fed notched UWB antenna designed for breast tumor detection applications," *Physica Scripta*, Vol. 100, No. 6, 065529, 2025.

[6] Bu, D., S.-W. Qu, and S. Yang, "Planar, ultra-wideband and dual-polarized phased array antenna for millimeter-wave vehicular communication," *IEEE Transactions on Vehicular Technology*, Vol. 73, No. 7, 9972–9983, 2024.

[7] Desai, A., H.-T. Hsu, B. M. Yousef, A. M. Ameen, Y.-F. Tsao, and A. A. Ibrahim, "UWB connected ground transparent 4-port flexible MIMO antenna for IoT applications," *IEEE Internet of Things Journal*, Vol. 11, No. 7, 12 475–12 484, 2024.

[8] Kakaraparty, K. and I. Mahbub, "High-gain, compact UWB antenna for wireless power transfer based wearable applications," *IEEE Open Journal of Antennas and Propagation*, 2024.

[9] Muhsin, M. Y., Z. S. Muqdad, A. H. Sahar, Z. F. Mohammad, and H. Al-Saedi, "Ultra-wideband antenna system design for future mmWave applications," *Journal of Telecommunications and Information Technology*, Vol. 1, 67–73, 2025.

[10] Zhao, L., Y. Wang, C. Liu, D. Song, C. Hu, C. Li, H. Zhao, and Z. Wang, "Compact circular-shaped MIMO antenna covers UWB bandwidth with four frequently-used band-notched characteristics for multi-scenario applications," *IEEE Access*, Vol. 12, 32 762–32 771, 2024.

[11] Platt, J. M., L. B. Boskovic, and D. S. Filipovic, "Wideband biconical antenna with embedded band-notch resonator," *IEEE Transactions on Antennas and Propagation*, Vol. 72, No. 3, 2921–2925, 2024.

[12] Sadineni, R. B., K. S. Rao, T. Sushma, P. V. K. Kanth, V. R. Rao, and D. P. Gowda, "Design of ultra-wideband antenna with quadruple band notch reconfigurability," *Progress In Electromagnetics Research C*, Vol. 144, 23–31, 2024.

[13] Al-Saedi, H., M. Y. Muhsin, Z. F. Mohammad, and W. M. Abdel-Wahab, "Ultra-wideband antenna array for modern millimeter-wave wireless applications," *Journal of Engineering and Sustainable Development*, Vol. 29, No. 5, 573–581, 2025.

[14] Ahmad, S., U. Ijaz, S. Naseer, A. Ghaffar, M. A. Qasim, F. Abrar, N. O. Parchin, C. H. See, and R. Abd-Alhameed, "A jug-shaped CPW-fed ultra-wideband printed monopole antenna for wireless communications networks," *Applied Sciences*, Vol. 12, No. 2, 821, 2022.

[15] Park, S. and K.-Y. Jung, "Novel compact UWB planar monopole antenna using a ribbon-shaped slot," *IEEE Access*, Vol. 10, 61 951–61 959, 2022.

[16] Khan, M. A., U. Rafique, H. S. Savci, A. N. Nordin, S. H. Kiani, and S. M. Abbas, "Ultra-wideband pentagonal fractal antenna with stable radiation characteristics for microwave imaging applications," *Electronics*, Vol. 11, No. 13, 2061, 2022.

[17] Kumar, N. N., B. S. Srikanth, S. B. Gurung, S. Manu, G. N. S. Gowthami, T. Ali, and S. Pathan, "A slotted UWB monopole antenna with truncated ground plane for breast cancer detection," *Alexandria Engineering Journal*, Vol. 59, No. 5, 3767–3780, 2020.

[18] Samadianfard, R., J. Nourinia, C. Ghobadi, M. Shokri, and R. Samadianfard, "A compact, ultra-thin UWB microstrip antenna for microwave imaging applications," *Soft Computing*, Vol. 27, No. 24, 19 113–19 124, Dec. 2023.

[19] Rani, P., M. K. Gaur, P. Tiwari, M. Kaushik, A. Shastri, and V. Gahlaut, "Design and implementation of a compact ultra-wideband reconfigurable antenna using RF MEMS switch technology," *Discover Electronics*, Vol. 2, No. 1, 32, Jun. 2025.

[20] Thaiwirot, W., J. Ardhan, S. Prengsri, P. Akkaraekthalin, and S. Chalermwisutkul, "The low-profile all-textile UWB antenna with AMC for WBAN Applications," *EURASIP Journal on Wireless Communications and Networking*, Vol. 2025, No. 1, 56, Jul. 2025.

[21] Devana, V. N. K. R., N. Radha, P. Sunitha, F. N. Alsunaydih, F. Alsaleem, and K. Alhassoon, "Compact MIMO UWB antenna integration with Ku band for advanced wireless communication applications," *Heliyon*, Vol. 10, No. 5, e27393, 2024.

[22] Saeidi, T., S. N. Mahmood, S. Saleh, N. Timmons, A. J. A. Al-Gburi, and F. Razzaz, "Ultra-wideband (UWB) antennas for breast cancer detection with microwave imaging: A review," *Results in Engineering*, Vol. 25, 104167, 2025.

[23] Cameron, R. J., C. M. Kudsia, and R. R. Mansour, *Microwave Filters for Communication Systems: Fundamentals, Design, and Applications*, John Wiley & Sons, 2018.

[24] Martínez-Lozano, A., C. Blanco-Angulo, H. García-Martínez, R. Gutiérrez-Mazón, G. Torregrosa-Penalva, E. Ávila Navarro, and J. M. Sabater-Navarro, "UWB-printed rectangular-based monopole antenna for biological tissue analysis," *Electronics*, Vol. 10, No. 3, 304, 2021.